# Dynamics of colloidal crystals in shear flow†

**Didi Derks,‡* Yu Ling Wu,§ Alfons van Blaaderen and Arnout Imhof**

*Received 12th September 2008, Accepted 1st December 2008*
*First published as an Advance Article on the web 3rd February 2009*
**DOI: 10.1039/b816026k**

We investigate particle dynamics in nearly hard sphere colloidal crystals submitted to a steady shear flow. Both the fluctuations of single colloids and the collective motion of crystalline layers as a whole are studied by using a home-built counter rotating shear cell in combination with confocal microscopy. Firstly, our real space observations confirm the global structure and orientation as well as the collective zigzag motion as found by early scattering experiments. Secondly, dynamic processes accompanying the shear melting transition are followed on the particle level. Local rearrangements in the crystal are seen to occur more frequently with increasing shear rate. This shear-enhanced particle mobility is quantified by measuring the random particle displacements from time-tracked particle coordinates. We find that shear induced melting takes place when these random displacements reach 12% of the particle separation, reminiscent of the Lindemann criterion for melting in equilibrium systems. In addition, a dynamic criterion for melting, based on the relative importance of the long time self diffusion compared to the short time self diffusion, is discussed.

## 1 Introduction

When does a crystal melt into a fluid? And how does shear flow affect this condition? In 1910 Lindemann addressed the first question: he proposed that as soon as the molecular fluctuations exceed ~10% of the intermolecular spacing, the order will be destroyed.[1] This Lindemann criterion was shown to also hold in colloidal crystals as has been demonstrated using computer simulation[2,3] and experiments.[3–5] In soft matter systems we have the possibility to easily modify the melting transition by applying external fields. In this work, we show that these fluctuations do not necessarily have to arise from an increase of thermal agitation, but are also increased by subjecting the crystal to shear flow. This eventually leads to complete shear induced melting of the 3D-crystal. The Lindemann melting criterion was already used in the context of shear flow by Lindsay and Chaikin,[6] who observed the shear melting transition through a sudden viscosity increase, and Ackerson and Clark who observed a reduction of long ranged order with light scattering.[7] However, the increased fluctuations were hypothesized rather than observed. More recently, Lindemann-like arguments were used to describe the phase behaviour of 2D-systems of magnetic particles.[8] In those experiments, the interparticle interaction could be directly tuned by the applied magnetic field strength, whereas the effect of shear flow is indirect and occurs *via* the interplay with the suspending fluid.

In the 1980s, the effect of shear flow on colloidal crystals was investigated extensively by means of light scattering techniques. In this way, the global structure and orientation of the sheared systems was obtained.[7,9–11] In the last decade the use of microscopy techniques became more established,[12–16] but real space investigations to study the effect of shear flow on the particle level in dense colloidal suspensions are not very numerous yet. Cohen and co-workers showed that strongly confined systems in shear flow gave rise to unexpected new crystal structures.[17] Also, shear banding was observed in dense colloidal crystals undergoing an oscillatory shear[18] and there were reports on the effect of a very low strain on the dislocation dynamics in colloidal crystals[19] and colloidal glasses.[20] Besseling *et al.* were the first to present a microscopy study on colloidal glasses undergoing steady shear.[21] A problem arising when studying a 3D system in a steady shear flow is that particles simply flow out of the field of view of the microscope, drastically limiting the time a particle can be followed (or be recognized to be the same particle). We circumvent this problem here by using a counter rotating shear cell in which a stationary layer can be positioned away from the glass wall.[13]

Shear melting has been found to occur in two stages: first there is the transition from a crystal in which the particle positions are bound to the 3D lattice sites to a situation in which (hexagonally ordered) layers slide more or less freely over each other.[9,13] The in-plane order is preserved until considerably higher shear rates, but will eventually vanish at higher shear rates as well. In this paper, we will first investigate this sliding layer motion and look at the collective displacement of particles in a layer. Second, we focus on how shear affects the random particle displacements and investigate how those increased fluctuations lead to the loss of crystalline order upon approaching the shear melting transition.

## 2 Experimental

We used rhodamine labeled poly(methylmethacrylate) (PMMA)-spheres with a diameter of 1.67 μm made by dispersion

*Soft Condensed Matter, Debye Institute for Nanomaterials Science, Utrecht University, Princetonplein 5, 3584 CC Utrecht, The Netherlands*

† Electronic supplementary information (ESI) available: Two movies of flow-vorticity plane under shear. See DOI: 10.1039/b816026k

‡ Present address: Laboratoire de Physique Statistique, Ecole Normale Supérieure, 24 rue Lhomond, 75231, Paris cedex 05, France. E-mail: didi.derks@lps.ens.fr

§ Present address: Department of Pharmaceutics, Utrecht Institute for Pharmaceutical Sciences, Utrecht University, Sorbonnelaan 16, 3584 CA, Utrecht, The Netherlands

 

polymerization and sterically stabilized by a layer of poly(12-hydroxystearic acid) (PHS).[22,23] The particles were dispersed in a 3 : 1 w/w mixture of cyclohexylbromide and *cis*-decalin, saturated with tetrabutylammoniumbromide (TBAB) yielding a nearly density and refractive index matched system in which the colloids behave nearly hard-sphere like ($\phi_{\mathrm{crystallisation}} = 0.47$).[24] A home-built counter rotating cone-plate shear cell was mounted on top of an inverted confocal microscope (Leica TCS SP2), where a 100 × 1.4 NA oil immersion objective was controlled by a piezo-focusing drive (Physik Instrumente P-721). The shear cell consists of a (replaceable) metal cone that makes an angle of either 1 or 4 degrees with a glass plate that has a diameter of 6.5 cm. The counter rotating principle allows us to locate the stationary layer (zero velocity plane) away from the lower glass wall. More details of the set up can be found in ref. 13. A pre-shear of 0.5 $s^{-1}$ was applied for 30 min to a dense suspension at a volume fraction of 0.57, well within the crystalline region of the phase diagram. The crystal was left to equilibrate for an additional hour, before starting the shear experiments described here. Time series were taken in the flow-vorticity (*xy*-) plane. The minimum capturing time of one frame was 0.26 s. Particle coordinates were determined using routines similar to those of Crocker and Grier.[25] Local shear rates were determined from flow profiles by measuring the velocity of about 10 consecutive layers around the zero velocity plane as explained in ref. 13. These profiles were always linear.

The importance of shear flow, which tends to distort the structure, in comparison to thermal motion, which tends to restore equilibrium structure, is usually expressed as the Péclet number $Pe = \eta\dot{\gamma}\sigma^3/k_{\mathrm{B}}T$.[26] Here $\eta$ is the viscosity of the solvent and $\sigma$ the particle diameter. For these experiments $Pe \approx (2.3\ \mathrm{s})\dot{\gamma}$.

## 3 Sliding layers

Filling the shear cell with the dense suspension results in a polycrystalline arrangement of random stacked hexagonally close packed (rhcp) crystals with the hexagonal layers parallel to the (horizontal) glass wall. The pre-shear treatment then aligns all the crystals such that in each *xy*-plane a close packed line points (within ±3°) in the direction of flow.[13] A typical resulting structure can be seen in the two confocal images in Fig. 1 for two different shear rates. These are snapshots from movies taken at approximately the eighth layer counted from the glass plate. Examples of time series obtained are provided as movies in the electronic supplementary information.† Time series of the hexagonal plane show that particles in the layers oscillate collectively in the vorticity direction. This is visualized in the graphs in the right part of Fig. 1. On the vertical axis we plotted in greyscale a histogram of the *y*-positions of all particles in the image. The peaks in the histogram are given a dark color and correspond to a high probability of finding a particle at that vertical position. The maxima correspond to the *y*-positions of rows of particles. This was done for each frame in the time series, resulting in wiggly lines. These oscillations imply that rows of particles oscillate in phase. The frequency of the oscillations increases with increasing shear rate.

To clarify the origin of this collective movement, additional data were taken by capturing a time series of an *xyz*-stack consisting of three *xy*-frames through the centers of particles in three

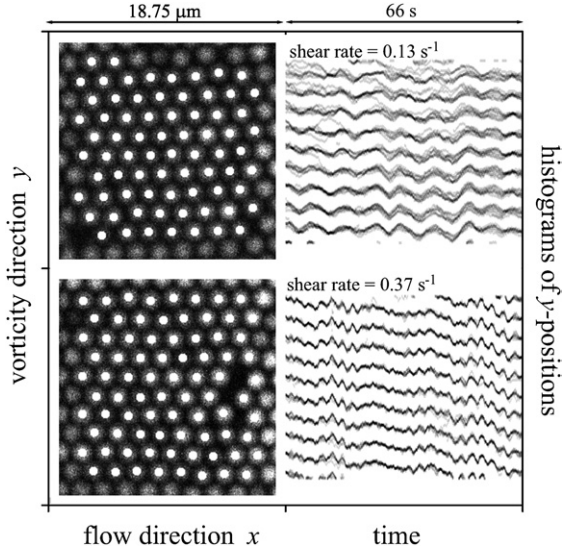


**Fig. 1** Visualization of the collective motion of hexagonally packed layers in shear flow. Images on the left show a snapshot at time $t = 0$ with the corresponding coordinates superimposed. On the right, we plot histograms in greyscale of the *y*-positions of particle rows along *x*. At each time a high grey value corresponds to a high probability of finding particles at that *y*-position. Top panels correspond to a shear rate of 0.13 $s^{-1}$, bottom panels correspond to 0.37 $s^{-1}$.

adjacent layers. In Fig. 2 (left), the particle coordinates of these three layers are plotted in one figure. From these figures it can be seen that the observed zigzag motion clearly is an effect that arises *via* interaction with particles in the neighboring layers. At this high volume fraction there is simply no space for layers to slide over each other in a straight line. As a result, particles follow zigzag paths through the saddles in the landscape formed by the adjacent layers. In each period of the oscillation the particles move collectively over a distance equal to one interparticle spacing of the adjacent layer. The oscillation frequency should then be proportional to the shear rate. This is confirmed in Fig. 3. First, the trajectory of the center of mass $r_{\mathrm{CM}}(t)$ of the particles is determined by accumulating the average displacement of particles appearing in two consecutive frames, up to time *t*:

$$\vec{r}_{\mathrm{CM}}(t) = \sum_{t'=\Delta t}^{t} \frac{1}{N_{t'}} \sum_{i=1}^{N_{t'}} \left(\vec{r}_i(t') - \vec{r}_i(t' - \Delta t)\right) \qquad (1)$$

Here, *i* runs over all $N_{t'}$ particles showing up in two subsequent frames, and $\Delta t$ is the time interval between those two frames. From this we then calculate the autocorrelation function of its component in the vorticity direction ($y_{\mathrm{CM}}$): $g_y(t) = \frac{1}{T}\int_0^T y_{\mathrm{CM}}(t')\, y_{\mathrm{CM}}(t'+t)\, \mathrm{d}t'$ where $T$ is the duration of the time series. Plotting this function against time normalized with the shear rate results in a nice overlap of the experiments at different shear rates. The shear rates used in this figure were measured independently by determining the velocity in *xy*-time series of ~10 layers around the studied layer.[13] The zigzag motion is still observed at a shear rate of 2.3 $s^{-1}$. At a shear rate of 3 $s^{-1}$ ($Pe = 7$) order was lost and the system was considered to have shear melted.

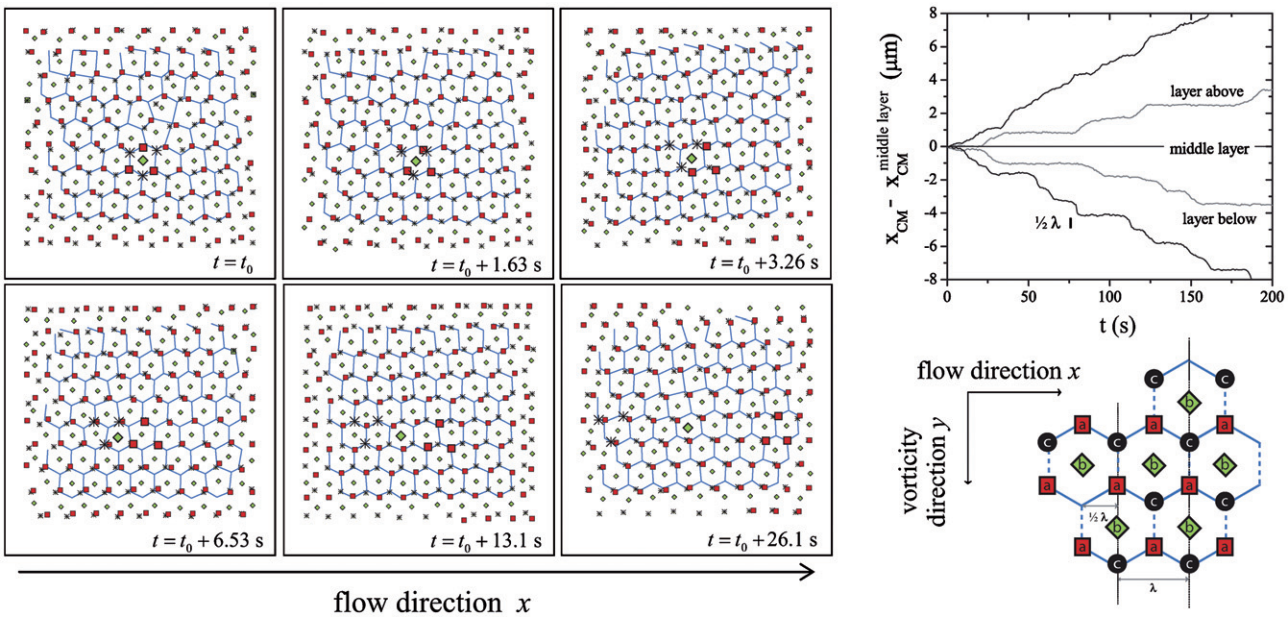


**Fig. 2** Collective motion in stacks of hexagonally packed layers in shear flow. (Left) Particle positions in three adjacent layers in shear flow ($\dot{\gamma} = 0.16$ $s^{-1}$) at six different times. A Voronoi construction of the middle layer (diamonds) is shown. Particles in the lower layer (stars) and upper layer (squares) are seen to neatly follow paths formed by the edges of the Voronoi cells. One particle in the middle layer and its neighbors at $t = t_0$ in the adjacent layers are highlighted for easier viewing. (Right) 'Stick-slip' motion at very low shear rate. Grey lines correspond to $\dot{\gamma} = 0.01$ $s^{-1}$, black lines to $\dot{\gamma} = 0.03$ $s^{-1}$. The position of the center of mass in the flow direction relative to the middle layer is plotted. Particles in adjacent layers reside at an 'a' or 'c' position (see sketch) for prolonged periods of time, and spend less time at intermediate positions. Each step, the layer moves over a distance of half the interparticle spacing $\lambda$ (0.9 μm).

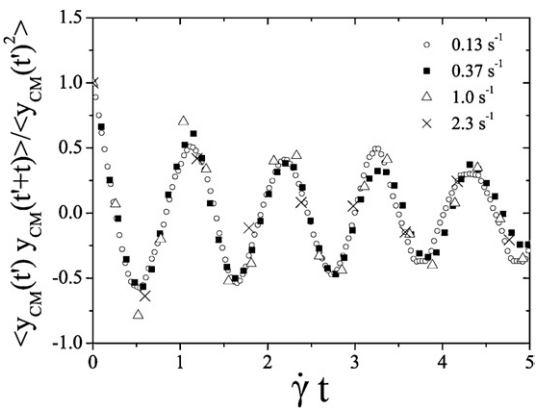


**Fig. 3** Zigzag motion in sheared colloidal crystals. Autocorrelation function of the $y$-coordinate of the center of mass, showing the oscillations of particles in the vorticity direction. Time is normalized with the independently measured (local) shear rate.

It is interesting that zigzag motion is still observed at the highest shear rate below melting. This is contrary to what has been observed in highly deionized suspensions under shear, where a gradual de-registering of layers with shear rate takes place.[27] This is probably due to the fact that in a hard sphere crystal there is simply not enough space for particles to forgo zigzagging. Similarly, elastic layer distortions[28] are of minor importance at these high packing fractions.

At very low shear rates ($Pe \ll 0.2$) the zigzag motion becomes difficult to detect. Particles spend most time at lattice sites formed by the adjacent layers. They avoid interstitial positions as much as possible, and hop to the next site only rarely. Still, when measuring over long enough times the hexagonal layers are seen to move relative to each other, and the velocity profile is on average linear. In the upper right corner of Fig. 2 we have visualized this 'stick-slip' motion by plotting the $x$-position of the center of mass relative to the middle layer as a function of time for three adjacent layers. It is seen that a particle moves over half an interparticle spacing at each jump. This corresponds to a move from an 'a' to a 'c' position. The jumps of the first and third layer are not necessarily in step. At higher shear rates the steps progressively smooth out.[13]

## 4 Fluctuations

Compared to the non-sheared case, in the sheared system particle rearrangements are more pronounced, vacancies travel more easily, and the individual particles are much less bound to their lattice positions. From the movies we observe that at a modest shear rate ($Pe = 0.3$), local order is occasionally lost, to be recovered later on (see ESI).† At increasing shear rate this occurs more frequently and also involves larger regions. Hints for such local (and temporal) loss of order can be seen in Fig. 1, for example in the lower snapshot on the righthand part of the image and in Fig. 2 at $t = t_0$ just above the highlighted particles. Interestingly, alternating cycles of order and disorder were also observed in simulations of Das *et al.*, in which (only) two superimposed layers were sheared.[29] To gain insight in the phenomenon of shear melting, and the conditions at which it occurs, we now focus on the random particle displacements that

 

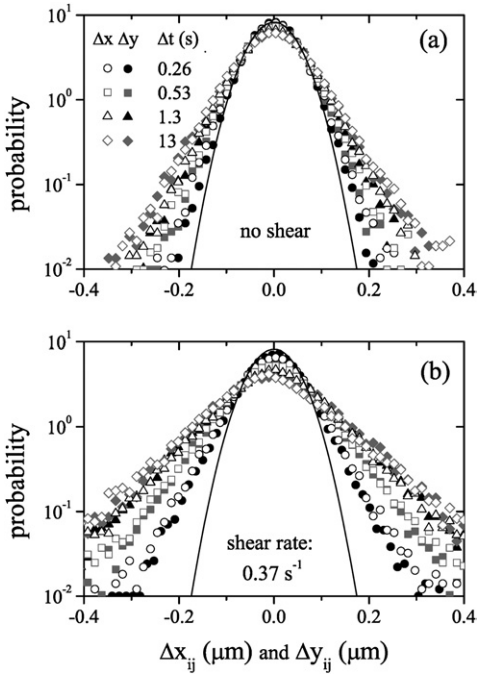


**Fig. 4** Histograms of the relative displacements in the $x$- and $y$-direction after different time intervals for an experiment at zero shear (a) and an experiment at a shear rate 0.37 $s^{-1}$ (b). Lines are Gaussian fits to the fluctuation distribution at the smallest time interval.

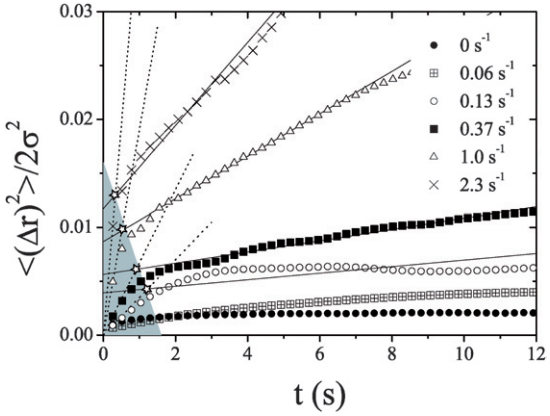


**Fig. 6** Mean square relative displacements in the flow-vorticity plane at different shear rates. The initial slope, given by dotted lines, is predominantly attributed to diffusion of particles around their lattice site, while at longer times particle rearrangements become the main contribution to diffusion. Stars mark the crossover between those two regions, thus defining a triangular region (shaded).

are present on top of the collective sliding layer motion discussed above. To remove the collective motion, we calculate the relative changes in the distance between pairs of neighboring particles instead of the absolute particle displacements,[8] because this focuses on the displacements relative to the lattice.

The vector between the positions of two neighboring particles is given by $\vec{r}_{ij} = \vec{r}_i - \vec{r}_j$, where $i > j$ are the indices of the neighboring particles. Each unique pair is given an identification number, so that the pair can be tracked in time. In this way a pair is followed for as long as the particles remain nearest neighbors (as calculated by a Delaunay triangulation). The displacements in time $t$ are then calculated for each pair according to $\Delta\vec{r}_{ij}(t) = \vec{r}_{ij}(t' + t) - \vec{r}_{ij}(t')$. Histograms of these relative displacements in both flow ($x$-) and vorticity ($y$-) direction are shown in Fig. 4 for different time intervals. The non-sheared system shows a narrow Gaussian distribution, which only slightly widens with time. In shear flow the distribution becomes broader. Also the shape of the distribution is changed: larger displacements occur more frequently than in a pure Gaussian distribution. This is in agreement with the observation that the increased fluctuations appear to be concentrated on a selection of the particles, while the others—which remain part of a crystalline patch—are much less affected. This phenomenon is illustrated in Fig. 5 and can also be seen from the Movies in the ESI.† In the first 13 s interval a large melted region is seen that has fully recrystallized by the time the second interval starts. In panels 4 and 5 different patches of the crystal are seen slipping with respect to each other.

In Fig. 6 the mean square relative displacement

$$\langle \Delta r^2 \rangle(t) = \langle \left( \vec{r}_{ij}(t + t') - \vec{r}_{ij}(t') \right)^2 \rangle \qquad (2)$$

is plotted as a function of time. Only the displacements in the flow-vorticity plane are taken into account; the displacement in the $z$-direction cannot be extracted from these $xy$-data. We normalized $\langle \Delta r^2 \rangle$ by $2\sigma^2$, where the factor 2 arises because we are interested in the mean square displacement per particle (and not per pair of particles).

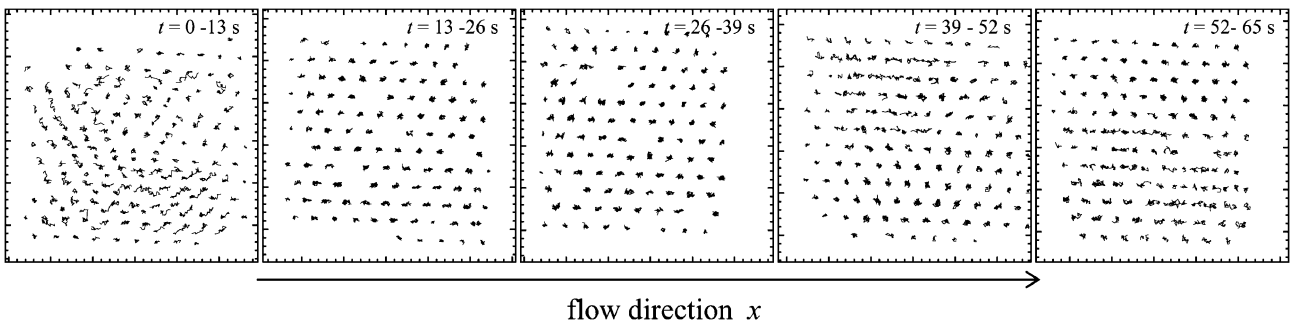


**Fig. 5** Particle tracks in the flow-vorticity plane over 13 s (50 frames) time intervals after subtraction of the average (zigzag) motion. The tracks show spatial and temporal heterogeneities in the fluctuations. The size of a panel is 22 × 22 $\mu m^2$ and the shear rate is 1.0 $s^{-1}$. Data correspond to Movie 2 in the ESI.†

It is seen that at zero shear the particles are strongly confined to their lattice site, so that their mean square displacement levels off to a finite value. Within the first few seconds, diffusion of the particles in a neighbor cage is observed, while at longer times the cage formed by the neighbors confines the particles. In the absence of shear the cage is static and particles cannot escape, at least on the time scale of our experiment. The sheared particles also feel their neighbors after the first (few) second(s), but apparently experience a more dynamic cage from which they still have a chance to escape. Interestingly, at long times the mean square displacement again increases approximately linearly with time.

The shaded part of Fig. 6 marks the region where particles still diffuse around their lattice site, before breaking out of their cages. At a shear rate of 2.3 $s^{-1}$ this takes less than half a second. On further increasing the shear crystalline order was lost at $\dot{\gamma} \approx 3$ $s^{-1}$. The shaded region intercepts the $y$-axis at a (relative) mean square displacement of 0.016. It is therefore clear from Fig. 6 that at the point of shear melting the mean square displacement of particles in their nearest-neighbor cages is approximately $\sqrt{\langle \Delta r^2 \rangle_{\mathrm{melt}}/2\sigma^2} \approx 0.12 \pm 0.01$. In other words, shear increases the random displacements of particles around their lattice positions until they exceed a value of about 0.12 times the lattice spacing, at which point the crystal shear melts. This is strongly reminiscent of a Lindemann criterion which in this case applies to a nonequilibrium system.[1,30] Hoffman and Löwen have found evidence for a Lindemann criterion in nonequilibrium simulations in which particles were driven in opposite directions.[31] To our knowledge, the present data provide the first experimental evidence.

Based on the arguments above, we can assign two self diffusion coefficients to the sheared systems: one that applies at short time scales, and another which applies at longer times. The best estimate we have for the short time self diffusion coefficient, is the value obtained from the displacements in the shortest experimentally measured time interval: $\langle \Delta r^2 \rangle/2 = 4D_{\mathrm{short}}\Delta t$, with $\Delta t =$ 0.26 s. At this time scale the colloids display essentially Brownian motion due to the many impacts of solvent molecules. In addition, at these high concentrations, particles influence each other by disturbing the flow field through which they move. Both the Brownian character of motion and the effect of hydrodynamic interactions are reflected in the short time self diffusion coefficient. The data obtained are shown in Fig. 7a. It is interesting to note that this *short time* diffusion coefficient already increases with the shear rate, and that it does so approximately linearly. Such behavior is exactly that seen in shear induced self diffusion of non-Brownian spheres, which is a purely hydrodynamic effect resulting from the hydrodynamic interactions between the ever-changing configurations of particles under shear.[32–34]

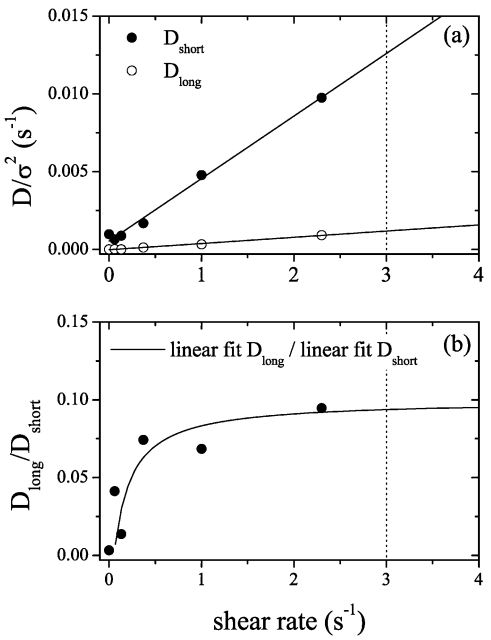


**Fig. 7** Short and long time diffusion coefficients in shear flow as obtained from Fig. 6. Complete shear melting occurs around a shear rate of 3 $s^{-1}$. This is indicated by the dotted line. The lines in (a) are linear fits to $D_{\mathrm{short}}$ and $D_{\mathrm{long}}$, respectively. The curve in (b) is the ratio of those fits.

At long time scales particles are slowed down further by direct particle–particle interactions. The long time self diffusion coefficient $D_{\mathrm{long}}$ is obtained from the linear slope of the long time mean square displacements. In Fig. 7a we plot these diffusion coefficients as a function of shear rate. Also, $D_{\mathrm{long}}$ increases linearly with shear rate. In part this will again be due to hydrodynamic effects. However, here direct interactions between particles also become more frequent with increasing shear rate and will add to the random displacements with an isotropic contribution that is proportional to the shear rate. This effect was observed in sheared suspensions of dilute but strongly interacting particles.[35] Another effect of shear flow, Taylor dispersion, gives a term quadratic in shear rate. However, it is not observed here because it is caused by particles leaving the layer in the gradient direction. These particles are not tracked.

In Fig. 7b it is seen that, relatively, $D_{\mathrm{long}}$ increases faster than $D_{\mathrm{short}}$. Near shear melting the long time diffusion coefficient is only a factor 10 times smaller than the short time diffusion coefficient. Interestingly, this ratio $D_{\mathrm{long}}/D_{\mathrm{short}} = 0.1$ was put forward by Löwen *et al.*[3] as a *dynamic* criterion for melting (again in equilibrium systems). This statement was based on the results of Brownian dynamics simulations, and was confirmed by experiments on low density colloidal systems of highly charged soft particles[3,36] and for slightly soft systems.[37] Though in these cases the hydrodynamic interactions are less important, the dynamic melting criterion was claimed to apply for concentrated systems where particles do interact through such interactions as well. By taking into account the short time diffusion coefficient which includes hydrodynamic interactions instead of the bare Stokes-Einstein diffusion coefficient, the experimental results for hard sphere crystallization described in ref. 38 could be explained. Our shear experiments indicate that this dynamic criterion for melting may well be applicable to non-equilibrium systems as well.

## 5 Conclusions

We have quantitatively studied colloidal crystals in shear flow in real space. We analyzed the collective zigzag motion that the particles perform when hexagonal layers are forced to slide over each other. On top of this collective motion the particles undergo random displacements. Random fluctuations are enhanced by

 

shear flow above those caused by Brownian motion. It was found that those fluctuations cause melting when they become sufficiently large. Similar to equilibrium systems, a Lindemann criterion accurately predicts the melting transition in these non-equilibrium systems. In addition, the data are consistent with a dynamic criterion based on the relative importance of the long time diffusion compared to the short time diffusion. Furthermore, we qualitatively observed that the path to shear melting is accompanied by local and temporary melting of the crystal. These fluctuations in the degree of crystalline order will be subject of future quantitative experimental investigations.

## Acknowledgements

The authors thank Hans Wisman, the "Instrumentele Groep Fysica (IGF)", and all participants in the design of the Wageningen Centre of Food Science (WCFS) shear cell. This work is part of the research program of the "Stichting voor Fundamenteel Onderzoek der Materie (FOM)", which is financially supported by the "Nederlandse Organisatie voor Wetenschappelijk Onderzoek (NWO)".

## References

1 F. A. Lindemann, *Physik. Zeitschr.*, 1910, **11**(14), 610.
2 M. J. Stevens and M. O. Robbins, *Phys. Rev. E*, 1993, **48**(5), 3778.
3 H. Löwen, T. Palberg and R. Simon, *Phys. Rev. Lett.*, 1993, **70**(10), 1557.
4 J. Bongers and H. Versmold, *J. Chem. Phys.*, 1996, **104**(4), 1519.
5 A. Brands, H. Versmold and W. van Megen, *J. Chem. Phys.*, 1999, **110**(2), 1283.
6 H. M. Lindsay and P. M. Chaikin, *J. Phys. (Paris) Colloque*, 1985, **46-C3**, 269.
7 B. J. Ackerson and N. A. Clark, *Phys. Rev. Lett.*, 1981, **46**(2), 123.
8 K. Zahn and G. Maret, *Phys. Rev. Lett.*, 2000, **85**(17), 3656.
9 B. J. Ackerson, *J. Rheol.*, 1990, **34**(4), 553.
10 S. Ashdown, I. Markovic, R. H. Ottewill, P. Lindner, R. C. Oberthür and A. R. Rennie, *Langmuir*, 1990, **6**(2), 303.
11 M. Tomita and T. G. M. van de Ven, *J. Colloid Interf. Sci.*, 1984, **99**(2), 374.
12 A. Imhof, A. van Blaaderen and J. K. G. Dhont, *Langmuir*, 1994, **10**(10), 3477.
13 D. Derks, H. Wisman, A. van Blaaderen and A. Imhof, *J. Phys.: Condens. Matter*, 2004, **16**, S3917.
14 R. Biehl and T. Palberg, *Rev. Sci. Instr.*, 2004, **75**(4), 906.
15 Y. L. Wu, J. H. J. Brand, J. L. A. van Gemert, J. Verkerk, H. Wisman, A. van Blaaderen and A. Imhof, *Rev. Sci. Instr.*, 2007, **78**(10), 103902.
16 M. Kogan, C. J. Dibble, R. E. Rogers and M. J. Solomon, *J. Colloid Interf. Sci.*, 2008, **318**(2), 252.
17 I. Cohen, T. G. Mason and D. A. Weitz, *Phys. Rev. Lett.*, 2004, **93**(4), 046001.
18 I. Cohen, B. Davidovitch, A. B. Schofield, M. P. Brenner and D. A. Weitz, *Phys. Rev. Lett.*, 2006, **97**(21), 215502.
19 P. Schall, I. Cohen, D. A. Weitz and F. Spaepen, *Nature*, 2006, **440**(7082), 319.
20 P. Schall, D. A. Weitz and F. Spaepen, *Science*, 2007, **318**(5858), 1895.
21 R. Besseling, E. R. Weeks, A. B. Schofield and W. C. K. Poon, *Phys. Rev. Lett.*, 2007, **99**(2), 028301.
22 G. Bosma, C. Pathmamanoharan, E. H. A. de Hoog, W. K. Kegel, A. van Blaaderen and H. N. W. Lekkerkerker, *Journal of Colloid and Interface Science*, 2002, **245**, 292.
23 L. Antl, J. W. Goodwin, R. D. Hill, R. H. Ottewill, S. M. Owens, S. Papworth and J. A. Waters, *Colloids and Surfaces*, 1986, **17**, 67.
24 A. Yethiraj and A. van Blaaderen, *Nature*, 2003, **421**(6922), 513.
25 J. C. Crocker and D. Grier, *J. Colloid Interf. Sci.*, 1996, **179**(1), 298.
26 R. G. Larson, *The Structure and Rheology of Complex Fluids*, Oxford University Press, Oxford, 1999.
27 R. Biehl and T. Palberg, *Europhys. Lett.*, 2004, **66**(2), 291.
28 B. J. Ackerson and N. A. Clark, *Physica A*, 1983, **118**, 221.
29 M. Das, S. Ramaswamy and G. Ananthakrishna, *Europhys. Lett.*, 2002, **60**(4), 636.
30 R. W. Cahn, *Nature*, 2001, **413**, 582.
31 G. P. Hoffmann and H. Löwen, *J. Phys.: Condens. Matter*, 2001, **13**(41), 9197.
32 V. Breedveld, D. van den Ende, M. Bosscher, R. J. J. Jongschaap and J. Mellema, *Phys. Rev. E*, 2001, **63**, 21403.
33 J. Acrivos, *J. Rheol.*, 1995, **39**, 813.
34 A. Sierou and J. F. Brady, *J. Fluid. Mech.*, 2004, **506**, 285.
35 X. Qui, H. D. Ou-Yang, D. J. Pine and P. M. Chaikin, *Phys. Rev. Lett.*, 1988, **61**(22), 2554.
36 R. Simon, T. Palberg and P. Leiderer, *J. Chem. Phys.*, 1993, **99**(4), 3030.
37 A. Imhof, A. van Blaaderen, G. Maret, J. Mellema and J. K. G. Dhont, *J. Chem. Phys.*, 1994, **100**(3), 2170.
38 A. van Blaaderen, J. Peetermans, G. Maret and J. K. G. Dhont, *J. Chem. Phys.*, 1992, **96**(6), 4591.